

Putative non-trivial topology in YNiSn₂ Dirac semimetal

G. S. Freitas^{1,2}, K. R. Pakuszewski^{1,4}, A. P. Machado¹, H. Pizzi¹, F. B. Carneiro^{2,3}, F. S. Oliveira¹, M. M. Piva⁵, E. M. Bittar^{2,3}, Y. Kopelevich¹, F. Ronning², J. D. Thompson², C. Adriano^{1,4}, and P. G. Pagliuso^{1,2}

¹*Instituto de Física Gleb Wataghin, UNICAMP, 13083-859, Campinas, SP, Brazil*

²*Los Alamos National Laboratory, Los Alamos, New Mexico 87545, USA.*

³*Brazilian Center for Research in Physics, Rio de Janeiro-RJ, Brazil.*

⁴*Univ. Montreal, Dept. Phys., Montreal, PQ H2V 0B3, Canada.*

⁵*Max Planck Institute for Chemical Physics of Solids, Nöthnitzer Str. 40, Dresden, Germany.*

(Dated: July 9, 2025)

In this work, we investigate the properties of single-crystalline YNiSn₂ through x-ray powder diffraction, elemental analysis, electrical resistivity, magnetic susceptibility, and specific heat measurements. YNiSn₂ crystallizes in an orthorhombic structure within the Cmcm space group (63), forming plate-like crystals with the *b* axis oriented out of the plane. The compound exhibits weak Pauli paramagnetism with a susceptibility of $\chi_0 = 2(3) \times 10^{-5}$ emu/mol-Oe and a small Sommerfeld coefficient of $\gamma = 4$ mJ/mol·K², indicating a low density of states at the Fermi level. Notably, at 1.8 K, YNiSn₂ displays a giant positive magnetoresistance of nearly 1000%, which increases quasi-linearly with the magnetic field up to $B = 16$ T, alongside a field-induced metal-insulator-like crossover under applied magnetic fields > 3 T. Furthermore, highly anisotropic dHvA quantum oscillations suggest a two-dimensional electronic band character from which a low effective mass and a high Fermi velocity could be extracted.

INTRODUCTION

Non-trivial topology in condensed matter physics has garnered significant interest over the past decades, driven by the discovery of new quantum phases of matter in systems such as topological insulators (TIs) in two or three dimensions, as well as Dirac and Weyl semimetals (DSMs and WSMs) [1–7]. Dirac semimetals are topological materials that host low-energy excitations resembling massless Dirac fermions. They have attracted considerable attention for studying relativistic quantum phenomena in condensed matter systems, which have promising applications in spintronics, quantum computing, and next-generation electronic devices. DSMs are notable for their exotic electronic bands, which linearly disperse in a three-dimensional momentum space through a nodal point (Dirac nodal point) near or at the Fermi level [5, 7]. This distinct characteristic gives rise to some of the most remarkable features of these materials, including exotic transport properties such as the chiral anomaly, large and non-saturating magnetoresistance, and exceptionally high carrier mobility [5, 8–11].

The non-trivial topology of a system's electronic bands has garnered significant attention in condensed matter physics, with TIs, DSMs, WSMs, and excitonic insulators (EIs) being subjects of intense investigation for decades due to either having fewer bands crossing the Fermi level or being completely gapped [12–17]. One particularly noteworthy feature observed in these classes of materials is the magnetic field-induced metal-to-insulator-like (M-I) transition [18–30]. It has been proposed [27] that an excitonic gap can be opened by a magnetic field in the linear spectrum of Coulomb-interacting quasiparticles in highly oriented pyrolytic graphite, closely analogous to

chiral symmetry breaking in the relativistic theories of (2+1)-dimensional Dirac fermions [28]. Similarly, theoretical studies have also proposed the M-I transition in Weyl semimetals [31].

The discovery of novel materials with intriguing electronic properties is highly desirable to further our understanding of the complex phenomena surrounding exotic semimetals, such as the examples mentioned above. In this context, we report in this work the physical properties of YNiSn₂ single crystals. This compound crystallizes in an orthorhombic crystal structure belonging to the space group Cmcm (63). At low magnetic fields, YNiSn₂ behaves as a semimetal with a low density of states at the Fermi level. However, at low temperatures, YNiSn₂ exhibits a giant positive magnetoresistance (MR) of nearly 1000 %, with a sub-linear field-dependent increase up to $B = 16$ T and a field-induced metal-insulator-like crossover. A magnetic field-induced thermal activation energy gap $\Delta \sim 0.3$ meV at $B = 16$ T was extracted for YNiSn₂.

Furthermore, our observations suggest that a 2D Fermi surface dominates the charge carrier behavior at low temperatures. Electronic bands with carriers exhibiting an effective cyclotron mass of $m^* = 0.085m_0$, where m_0 is the free electron mass, were extracted from de Haas-van Alphen (dHvA) oscillations detected for the applied magnetic field along the *b* axis, indicating anisotropic Fermi surfaces. A small area of such a Fermi surface indicates nodal-like pockets at the Fermi level. Moreover, Initial angle-resolved photoemission spectroscopy (ARPES) (manuscript in preparation) has revealed interesting features that may be associated with the presence of surface states, Dirac cones, and Fermi arcs in the band structure of YNiSn₂.

EXPERIMENT

Single crystalline samples of YNiSn_2 were grown by the Sn-flux method. High-purity elements of Y, Ni, and Sn, with the stoichiometry 1:1:20, were placed inside an alumina crucible and sealed in an evacuated quartz tube. The sample was heated in a furnace with a rate of 100°C/h up until 1100°C and kept at this temperature for 12 h. In sequence, the tube was slowly cooled down at 2°C/h to 900°C , followed by a faster cool down to 550°C . Then, the batches were removed from the furnace and placed into a centrifuge to separate the crystals from the flux. This growth method yielded nice platelet-like single crystals with typical $0.5\text{ mm} \times 0.5\text{ mm} \times 0.1\text{ mm}$ dimensions. Moreover, the synthesized phase stoichiometry for our YNiSn_2 single crystals was determined to be very close to the 1-1-2 (within 3%) by elemental analysis using energy dispersive x-ray spectroscopy (EDS).

Magnetization measurements were performed in a Quantum Design magnetic properties measurement system (MPMS3) equipped with a 7 T magnet. Specific heat measurements were done in a small-mass calorimeter system that employs a quasi-adiabatic thermal relaxation technique. In-plane electrical resistivity was obtained in a commercial AC-frequency bridge using the standard four-probe technique and with the current applied in the crystal plates. These measurements were performed in a commercial physical property measurement system (PPMS) cryostat of Quantum Design with a 16 T magnet. Powder and single-crystal x-ray diffraction were performed using a Panalytical Empyrean powder diffractometer with $\text{Cu-K}\alpha$ radiation and a Bruker D8 Venture single-crystal diffractometer equipped with $\text{Mo-K}\alpha = 0.71073\text{ \AA}$ radiation, respectively. The crystallographic orientation of the single crystals was determined using a real-time Laue X-ray system.

ARPES preliminary low-stats experiments were performed at the Canadian Light Source (CLS), using Scienta-Omicron R4000 in fixed energy mode with a Pass Energy = 20 eV. Incident photon energies of $E_i = h\nu = 60\text{ eV}$ and 120 eV were employed at $T = 13\text{ K}$. Samples were cleaved *in-situ* perpendicular to the (010)-direction with a pressure better than $5 \times 10^{-11}\text{ mbar}$.

RESULTS AND DISCUSSION

An orthorhombic crystal structure with $Cmcm$ (63) space group and lattice parameters $a = 4.409\text{ \AA}$, $b = 16.435\text{ \AA}$, $c = 4.339\text{ \AA}$ for our single crystals of YNiSn_2 was confirmed by x-ray powder and single crystal diffraction at room temperature using commercial diffractometers. Figure 1 displays the obtained crystalline structure. The $CmCm$ phase is in contrast with the $Pnma$ orthorhombic crystal structure proposed for YNiSn_2 in the Materials Project Initiative (mp-21981) and previously

found for polycrystalline samples of YNiSn_2 [32, 33]. In fact, our results are consistent with the structure previously found for polycrystalline of $R\text{Ni}_{1-x}\text{Sn}_2$ ($R = \text{La, Ce, Pr, Nd, Sm}$) [33–36] and CeNiSn_2 [37]. It is important to highlight that, considering the Ni vacancies found in this family, we measured EDS on several different single crystals and attempted to search for vacancies in the single-crystal X-ray diffractogram refinement. The stoichiometry of 1:1:2 was confirmed.

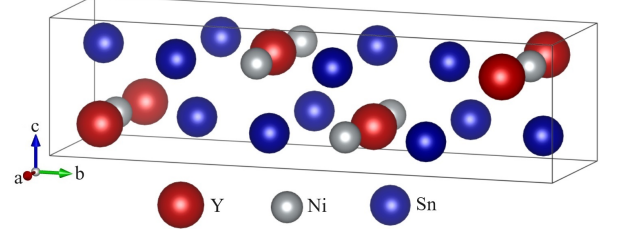


Figure 1. Crystalline structure of YNiSn_2 .

Figure 2 presents the zero magnetic field a) specific heat (c_p) and b) electrical resistivity (ρ) as a function of temperature for YNiSn_2 . The specific heat data in the temperature range between $0.4\text{ K} < T < 6\text{ K}$ was fitted by the expression $c/T = \gamma + \beta T^2$ as seen in the inset of Figure 2a). The fitting parameters obtained from these data are $\gamma = 4.0(5)\text{ mJ/mol}\cdot\text{K}^2$ and $\beta = 0.41(2)\text{ mJ/mol}\cdot\text{K}^4$, indicating a small density of states.

Assuming a free conduction electron gas model for YNiSn_2 , $\gamma = (2/3)N\pi^2k_B^2\eta(E_F)$ [38], we calculate the zero field/low-T density of states at the Fermi level, $\eta(E_F) = 0.83(4)\text{ states/eV mol-spin}$ from the obtained Sommerfeld coefficient. From $\beta = \frac{12\pi^4 Nk_B}{5\theta_D^3} \cong 1944/\theta_D^3$ [38], we extracted a Debye temperature θ_D of $\approx 170\text{ K}$.

The inset of Figure 2b) presents a zoomed-in plot of $\rho(T)$ measured under applied magnetic fields of 0 T and 0.1 T parallel to the b -axis, revealing a distinct kink at around 3.7 K. This kink originates from the superconducting transition of residual Sn at 3.72 K [39].

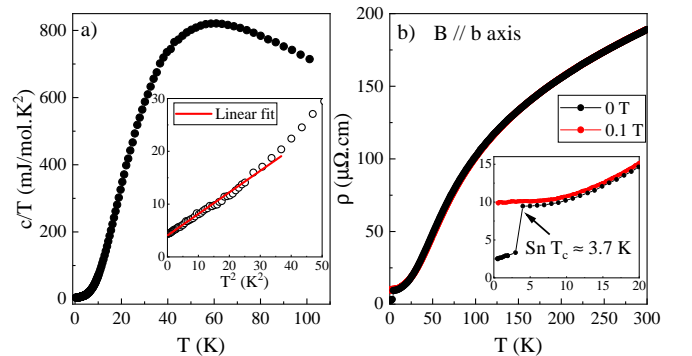


Figure 2. Zero-Field temperature dependence of a) specific heat and b) dc resistivity for YNiSn_2 .

Figure 3a) shows the in-plane magnetic transport data $\rho(T, B)$ for YNiSn₂ for a magnetic field applied perpendicular to the ac -plane. The resistivity shows a strong response to the magnetic field, with a positive magnetoresistance MR = 1000 % achieved at $T = 2$ K under a magnetic field of $B = 15$ T. As one can observe, under an applied magnetic field, $\rho(T)$ follows a metallic-like behavior down to a temperature scale where the resistivity shows a minimum, indicating a field induced Metal-Insulator-like (M-I) crossover. This behavior resembles the $\rho(T, B)$ data previously obtained by the magneto-transport measurements on the Weyl semimetal TaAs [40].

Thus, Figure 3 b) shows the first derivative of the $\rho(T)$ data for different magnetic fields presented in Figure 3a). In these data, it is possible to identify two important temperature scales: i) T_{MI} , which marks the onset of the M-I-crossover, below which $\rho(T)$ displays an insulating behavior and ii) T_p , which defines the temperature of the inflection point below which a saturation plateau develops on the $\rho(T)$. Interestingly, both T_{MI} and T_p increase monotonically with the magnetic field, as displayed in Figure 3c).

A thermal activation transport $\rho(T) \propto \exp(\Delta/k_B T)$ can be used to analyze the temperature-dependent resistivity below T_{MI} for YNiSn₂. The thermal activation energy (Δ) can then be extracted from the slope of the $\ln\rho(T)$ versus $1/T$ curves, as shown in Figure 3d). The linear fit presented in 3d) was performed between T_{MI} and T_p of each applied magnetic field $\rho(T)$ data (Figure 3c). The extracted Δ increases monotonically with the applied magnetic, as can be noted in Figure 3e). For $B > 10$ T, Δ seems to saturate in a value of ≈ 2.8 K (or 0.25 meV). This extracted thermal activation energy gap Δ at $B = 15$ T for YNiSn₂ is two order of magnitudes smaller than that for TaAs (≈ 29 meV at 9 T) and for others semimetallic systems, such as LaBi ($\Delta \sim 4.5$ meV), LaSb ($\Delta \sim 6.3$ meV) and LaSbTe ($\Delta \sim 1.9$ meV) [40].

Notably, T_{MI} seems to follow a tendency of $\approx B^{1/2}$, as observed in Figure 3c). This behavior agrees with the one proposed by Khveshchenko related to an excitonic gap in a Dirac semimetal [27]. He has shown that the applied magnetic field induces a gap opening, driving the system to an excitonic insulator phase, thus gapping up the quasiparticle spectrum of the Dirac fermions. This can be further explored in YNiSn₂.

The temperature-dependent magnetic susceptibility $\chi(T)$ data for single crystals of YNiSn₂ is presented in Figure 4. All YNiSn₂ samples present a weak temperature dependence magnetic susceptibility for which the sign is field-dependent. For the density of states $\eta(E_F) = 0.83(4)$ states/eV mol-spin extracted from the zero field heat capacity data of Figure 2, one would expect an electronic spin susceptibility of $\chi_e = 2\mu_B^2\eta(E_F) \approx 0.07 \times 10^{-4}$ emu/mol.Oe, which is in agreement with low

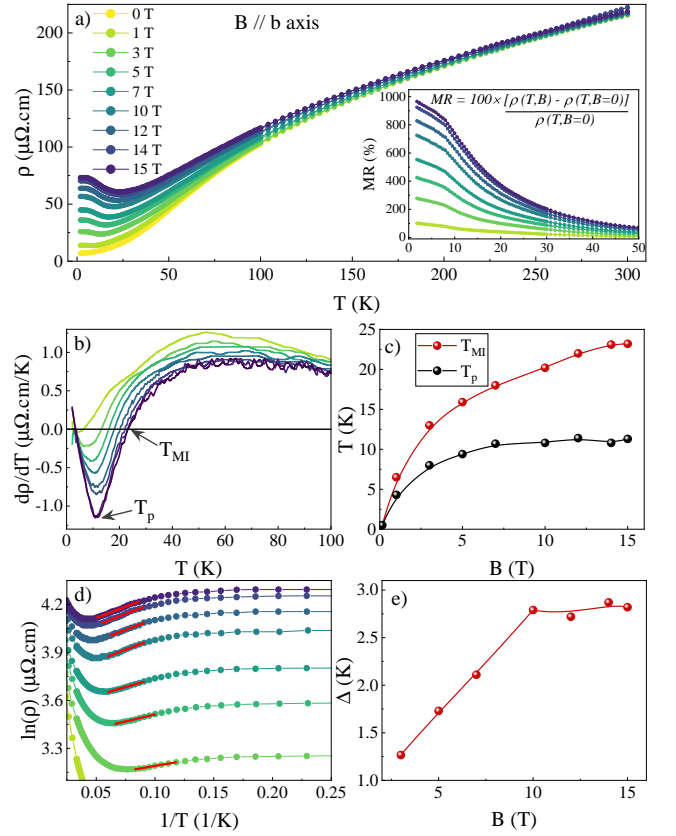


Figure 3. a) In-plane magnetic transport data $\rho(T, B)$ for YNiSn₂ with a magnetic field applied perpendicular to the plane. In the inset in a), we present the magnetoresistance (MR) as a function of the temperature. b) The derivative of $\rho(T, B)$ as a function of the temperature, wherein we present the discussed in the text T_{MI} and T_p . c) The behavior to T_{MI} and T_p as a function of the applied magnetic field. d) $\ln\rho$ as a function of T^{-1} yielding a thermal activation energy gap for different magnetic fields. e) Thermal activation energy (Δ) as a function of magnetic field.

field $\chi(T)$ data of YNiSn₂ (see Figure 4a)). However, the $\chi(T)$ data of YNiSn₂ become strongly diamagnetic and weakly anisotropic at high fields, as shown in Figure 4b).

Figure 5a) shows the magnetization versus the magnetic field applied parallel/perpendicular to the b axis up to $B = 6.5$ T for several temperatures ranging from 1.8 to 20 K. The data clearly display de Haas-van Alphen (dHvA) oscillations that become more evident after subtracting the high- T diamagnetic contribution, as shown in Figure 5b). Interestingly, the dHvA oscillations couldn't be observed for the magnetic field applied along the ac plane, suggesting that these oscillations originate from a very anisotropic Fermi surface. Figure 5c) presents the fast-Fourier transform (FFT) spectrum in which two very close distinguishable frequencies at $F_1 = 43.5$ T and $F_2 = 60.8$ T were observed. It is important to point out that although several oscillation frequencies

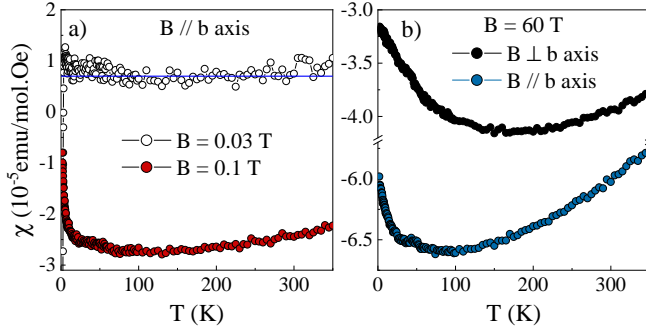


Figure 4. Temperature dependent magnetic susceptibility $\chi(T)$ data for single crystals of YNiSn₂. a) For fields of 300 Oe and 1 kOe applied along the b axis; b) Anisotropic behavior of $\chi(T)$ when a field of 6 kOe is applied parallel and perpendicular of the b axis.

for different orientations can be found in the pure Sn, its frequency ranges from 170 T to 10^5 T, much larger than the two frequencies observed for YNiSn₂ [41, 42].

Based on the Onsager relation, $F = (\Phi_0/2\pi^2)A_F$, where A_F is the cross-section area of the Fermi surface normal to the applied magnetic field, we extracted an estimated value of $4.1 \times 10^{-3} \text{ \AA}^{-2}$ for frequency 43.5 T. This A_F corresponds to about 1% of the total area of the Brillouin zone basal plane ($\approx 0.44 \text{ \AA}^{-2}$), suggesting that dHvA oscillations arise from a small Fermi pocket. By assuming a circular cross-section, we can extract a Fermi wave vector of $k_F = (A_F/\pi)^{1/2} = 0.034 \text{ \AA}^{-1}$.

The nature of the carriers participating in quantum oscillations can be revealed from further quantitative analyses of the dHvA oscillations. If the higher harmonic frequency is not significant, the oscillatory magnetization amplitude (ΔM) can be described using the Lifshitz-Kosevich formula: [18, 40, 43]

$$\Delta M \propto B^{1/2} R_T R_D \cos[2\pi(\frac{F}{B} + \gamma - \delta)] \quad (1)$$

where

$$R_T = \alpha T \mu / [B \sinh(\alpha T \mu / B)], \quad (2)$$

$$R_D = \exp(-\alpha T_D \mu / B) \quad (3)$$

From the fits to the temperature dependence of the FFT amplitude to the thermal damping factor R_T (Figure 5 d) we extracted the effective cyclotron mass of $m^* \approx 0.057 m_0$ for both F_1 and F_2 , where m_0 is the free electron mass. The value of the magnetic field used in this fit was the average inverse field value of the FFT window analyzed, with m^* and a prefactor as free parameters. The very small effective mass obtained suggests a Fermi surface with linear dispersion, such as the ones observed in Dirac and Weyl semimetals [7, 18]. Additionally, from the found effective mass, we can extract a Fermi velocity $v_F = \hbar k_F / m^* = 6.9 \times 10^5 \text{ m/s}$ for the YNiSn₂ single

crystals. This value of v_F is comparable to other compounds identified as possible Dirac semimetals, such as ZrSiS [25], TaAs [40], BaMnBi₂ [44], TlBiSSe [45], among others.

Furthermore, by fitting the field dependence of the oscillation amplitude normalized by R_T to R_D (Figure 5e), we found $T_D = 4.7 \text{ K}$ and $T_D = 3.8 \text{ K}$ for F_1 and F_2 , respectively. Thus, using $T_D \sim 4 \text{ K}$, the corresponding electron scattering time ($\tau = \hbar/2\pi k_B T_D$) is roughly $3.6 \times 10^{-13} \text{ s}$. This small T_D and consequent long scattering time indicate a high-quality single crystalline sample that facilitates the observation of the oscillations.

Figure 6a) presents the in-plane magnetoresistance $MR = (\rho(B) - \rho(B = 0))/\rho(B = 0) \times 100\%$ data for YNiSn₂ when the magnetic field is applied perpendicular to the ac plane. These data revealed a positive magnetoresistance of nearly 1100% achieved at $T = 1.8 \text{ K}$ under a magnetic field of $H = 16 \text{ T}$. Moreover, Shubnikov-de Haas (SdH) quantum oscillations under high magnetic fields can be observed. However, due to the small signal-to-noise ratio of the SdH oscillations, which could lead to misleading values for the frequencies and effective mass, a complete analysis was not possible. Improved measurements with a lower signal-to-noise ratio and with higher applied magnetic fields will be performed on YNiSn₂.

By fitting MR field dependence with a power law, we found $MR \propto B^n$ with $n = 0.72(3)$, close to a square-root dependence. In fact, as presented in Figure 6b), it was observed a crossover of a low field region displaying a linear dependence and the high field region with a $B^{1/2}$ dependence. Interestingly, a very similar behavior of the MR was theoretically described to appear in certain quasi-2D layered metals [46]. This could occur when the separation between Landau levels significantly exceeds the width of these levels and the interlayer interactions within the material. The emergence of the square-root dependence of MR is attributed to short-range (point-like) interactions with impurities, leading to changes in the effective scattering rate of electrons when subjected to a magnetic field. This effect is expected in materials where the quantized motion of electrons and their interactions with lattice imperfections are significant [46, 47]. To the best of our knowledge, no 3D material has been found that presents such MR crossover behavior. Curiously, a very similar theoretical study was performed in disordered graphene wherein it predicted a square-root MR at high fields [48]. This was observed experimentally in a graphene monolayer [49]. For more details, one can take a look at references [46–49] and references therein. The potential explanation for the observed MR behavior in YNiSn₂ as a characteristic of quasi-2D layered metals needs further exploration.

Additionally, in the low-field regime, the observed linear scaling of MR with the magnetic field is a distinctive feature of Landau quantization, which is characteristic of quasi-2D or Dirac-like systems in magnetic

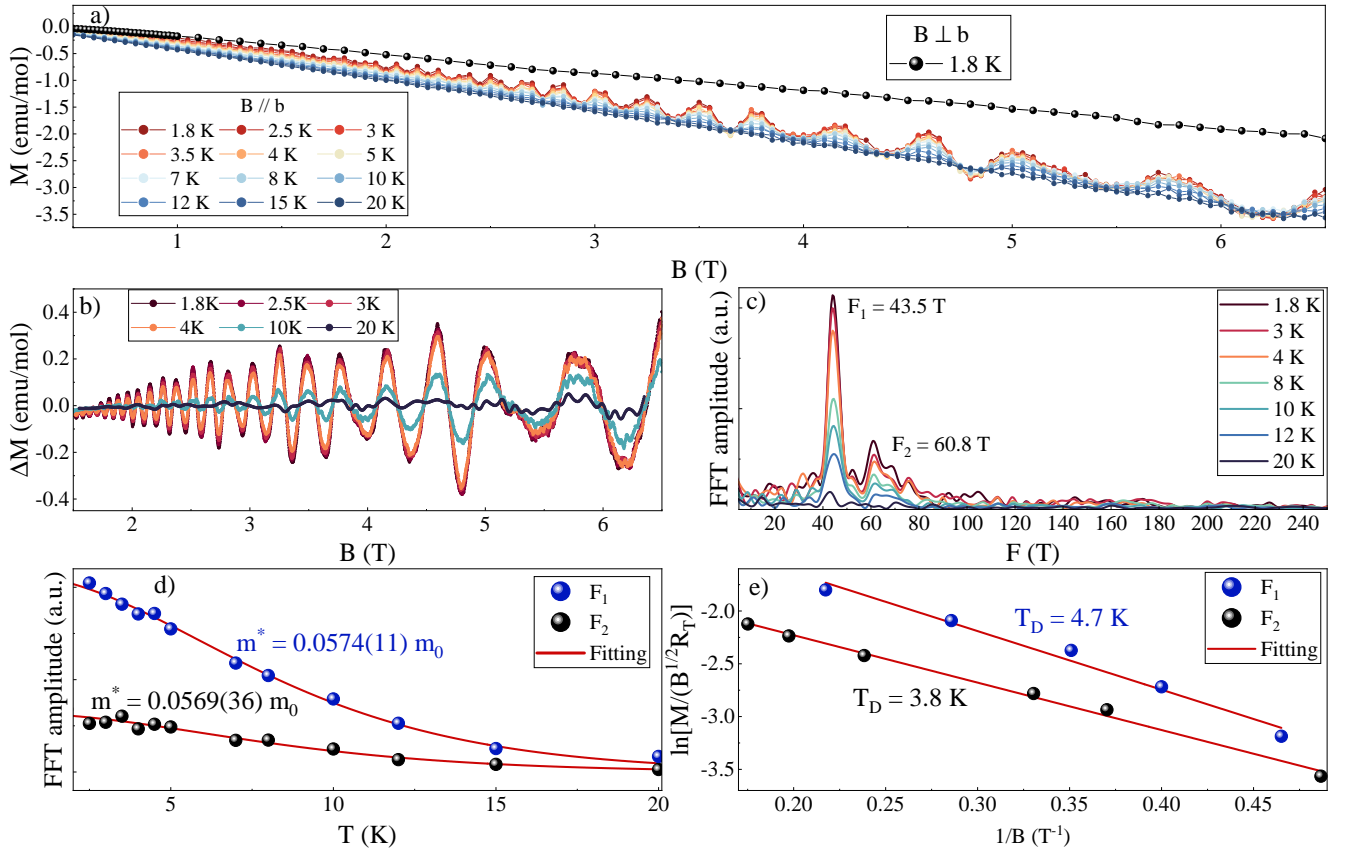


Figure 5. a) YNiSn₂ magnetization data versus magnetic field applied parallel/perpendicular to the plane up to $B = 6.5$ T for several temperatures ranging from 2 to 20 K. The data clearly display dHvA oscillations for B parallel to the b -axis, which become more evident after subtracting the high- T diamagnetic contribution (b). c) Fast-Fourier transform (FFT) spectrum of the ΔM data for several temperatures ranging from 2 to 20 K. Analysis of the ΔM to extract m^* (d) and T_D (e).

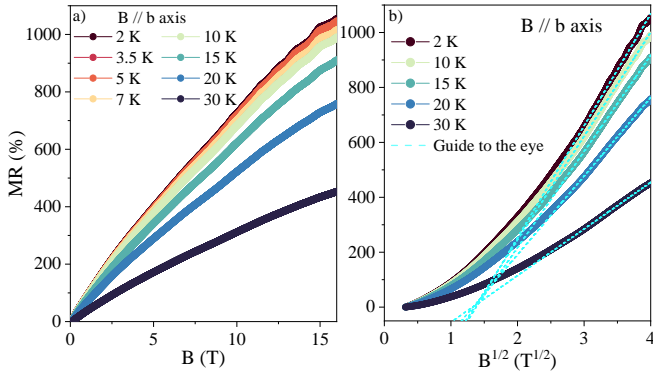


Figure 6. a) Magnetoresistance as a function of the applied field along the b axis. b) MR as a function of the square root of the applied field.

fields [50]. In fact, as we display in Figure 7, the MR data is best described by an exponential dependence $MR \propto \exp[-B_0/B]$, where B_0 is a temperature-dependent parameter. This relationship indicates that low-field MR behavior is governed by the characteristic

magnetic length scale $l_B = (\hbar/eB)^{1/2}$, which influences the localization and occupation of edge states in low-dimensional systems [51]. Supporting this, the inset in Figure 7 reveals that the B_0 parameter exhibits an inverse temperature dependence. This unusual exponential response to the magnetic field and its temperature scaling align with a Kosterlitz-Thouless-type correlation length (KT), as indicated in the Figure 7 inset. This observed KT correlation length is another particular signature of quasi-2D behavior [52]. Therefore, the presented findings suggest the presence of surface states and quasi-2D behavior in the YNiSn₂ compound. The origin of this unusual low-field MR likely originates from quantum interference effects in low-dimensional systems [53].

On this matter, we performed measurements of MR as a function of the applied magnetic field, as displayed in Figure 8. Similar to the behavior observed in the magnetization (Figure 5a), the quantum oscillations are suppressed when the magnetic field is applied perpendicular to the b axis, suggesting that the electronic band responsible for these oscillations has a quasi-2D Fermi surface character. In Figure 8, it can be observed that the MR

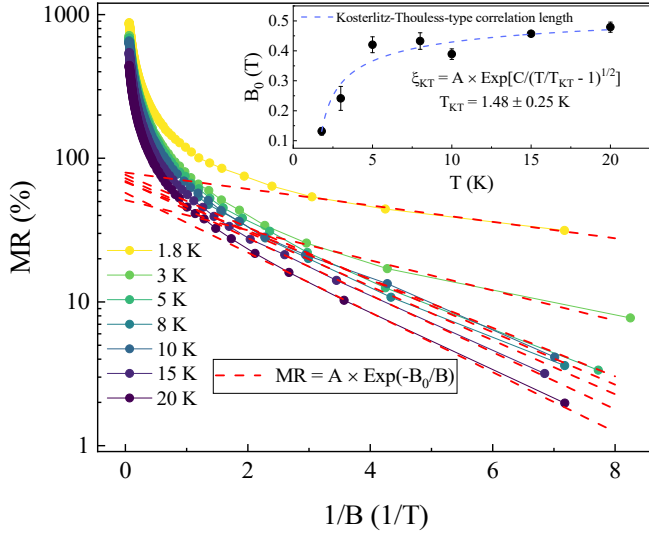


Figure 7. Magnetoresistance versus magnetic field inverse for temperatures ranging from 1.8 K up to 20 K. Dash red lines are fittings using the $MR \propto \exp[-B_0/B]$ relation. The inset shows the B_0 parameter temperature dependence. The blue dash line is the Kosterlitz-Thouless type correlation length that diverges exponentially.

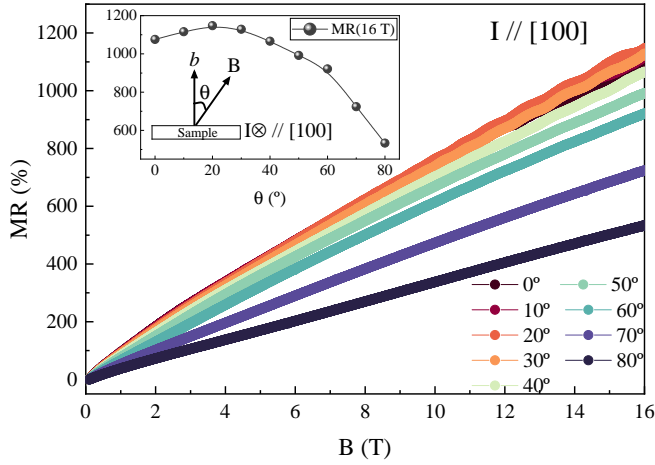


Figure 8. Magnetoresistance as a function of the applied magnetic field at different angles with respect to the b axis. The inset shows the MR at $B = 16$ T as a function of the angle.

reaches its maximum value of 1150% around $\theta = 20^\circ$, with θ being the angle between the applied magnetic field and the b axis, as illustrated in Figure 8. For $\theta > 20^\circ$, the MR at 16 T decreases monotonically to the value of 530% at $\theta = 80^\circ$, where no SdH oscillation can be observed.

Furthermore, initial ARPES measurement has revealed structures of linear dispersion near the Fermi level, as show in Figure 9, agreeing with the discussed behavior in this work. Figure 9 presents the ARPES band maps at isoenergetic surfaces for photon energies of $h\nu = 120$ eV and 60 eV at a temperature of $T = 13$ K. The cuts along the Fermi surfaces of YNiSn_2 are marked by solid

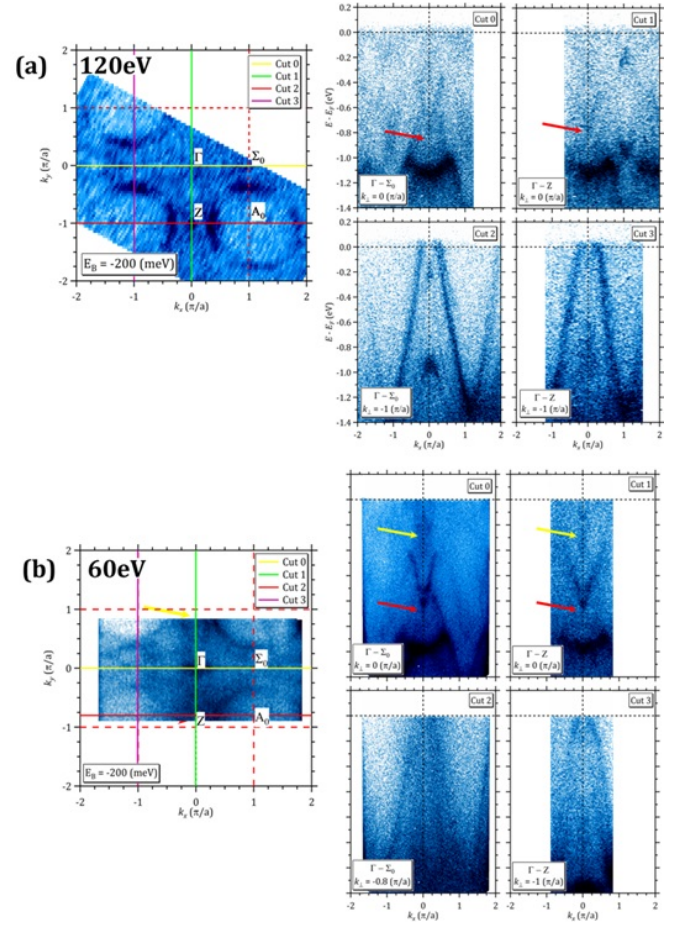


Figure 9. ARPES Band Maps along several Fermi surface cuts for $E_i = 120$ eV and 60 eV at $T = 13$ K for YNiSn_2 .

lines. Panel (a) shows the 120 eV data, while panel (b) displays the 60 eV data. The isoenergetic surfaces are integrated over an energy range of $\Delta E = \pm 20$ meV for a binding energy of $E_B = E_F = -200$ meV. Key Brillouin Zone points (Γ , Σ_0 , A_0 , and Z) are labeled in the plots.

In the 60 eV band map along the $\Gamma - \Sigma_0$ direction (cut 0), a cone-like structure with a V-shaped dispersion appears near the Fermi level (yellow arrow) but is absent in the 120 eV map. Additionally, two more cone-like structures, one V-shaped and one wedge-shaped, intersect around an energy of approximately $E_B = -750$ meV, as indicated by red arrows in Figures 9a and b. Further experiments and analysis are being done to describe the band structure of this compound.

CONCLUSIONS AND PERSPECTIVES

In summary, we performed x-ray diffraction, elemental analysis, electrical resistivity, magnetic susceptibility, and specific heat measurements on newly synthesized single crystals of YNiSn_2 . This compound crystallizes in

an orthorhombic structure with lattice parameters $a = 4.409 \text{ \AA}$, $b = 16.435 \text{ \AA}$, and $c = 4.339 \text{ \AA}$, belonging to the $Cmcm$ (63) space group. Our results indicate a weak Pauli paramagnetic susceptibility and a small Sommerfeld coefficient in the electronic heat capacity, consistent with a low density of states at the Fermi level.

Transport measurements reveal a field-induced metal-insulator-like transition above 3 T, accompanied by a giant positive magnetoresistance of nearly 1000% at $T = 1.8 \text{ K}$. The crossover between linear and square-root field dependencies suggests a two-dimensional character of the Fermi surface, further supported by the highly anisotropic magnetoresistance and SdH oscillations.

Additionally, pronounced dHvA quantum oscillations were observed, with analysis yielding a small effective mass, a low Fermi surface cross-section, and a high Fermi velocity—indicative of a quasi-linear energy dispersion. Initial ARPES measurements also reveal cone-like features, reinforcing this picture. While these findings highlight intriguing electronic properties, further experiments are required to achieve a comprehensive understanding of YNiSn_2 .

ACKNOWLEDGMENTS

We thank Sean M. Thomas and Priscila Rosa for the support and useful discussions. This work was supported by FAPESP (Grants No 2015/09701-7, 2017/10581-1, 2012/04870-7, 2012/05903-6, 2018/11364-7, 2020/12283-0), CNPq (Grants No. 311783/2021-0, 309483/2018-2, 314587/2021-7, 442230/2014-1 and 304649/2013-9), CAPES and FINEP-Brazil. The authors would like to acknowledge the Brazilian Nanotechnology National Laboratory (LNNano Project Inspect, 14958) for providing the equipment and technical support for the experiments involving scanning electron microscopy. Work at Los Alamos National Laboratory was performed under the auspices of the U. S. Department of Energy, Office of Basic Energy Sciences, Division of Materials Science and Engineering.

-
- [1] B. A. Bernevig, T. L. Hughes, and S.-C. Zhang, Quantum Spin Hall Effect and Topological Phase Transition in HgTe Quantum Wells, *Science* **314**, 1757 (2006).
 - [2] M. König, S. Wiedmann, C. Brüne, A. Roth, H. Buhmann, L. W. Molenkamp, X.-L. Qi, and S.-C. Zhang, Quantum Spin Hall Insulator State in HgTe Quantum Wells, *Science* **318**, 766 (2007).
 - [3] D. Culcer, A. C. Keser, Y. Li, and G. Tkachov, Transport in two-dimensional topological materials: recent developments in experiment and theory, *2D Materials* **7**, 022007 (2020).
 - [4] M. Z. Hasan and C. L. Kane, *Colloquium* : Topological insulators, *Reviews of Modern Physics* **82**, 3045 (2010).
 - [5] B. Yan and C. Felser, Topological Materials: Weyl Semimetals, *Annual Review of Condensed Matter Physics* **8**, 337 (2017).
 - [6] C. Zhang, H.-Z. Lu, S.-Q. Shen, Y. P. Chen, and F. Xiu, Towards the manipulation of topological states of matter: a perspective from electron transport, *Science Bulletin* **63**, 580 (2018).
 - [7] N. Armitage, E. Mele, and A. Vishwanath, Weyl and Dirac semimetals in three-dimensional solids, *Reviews of Modern Physics* **90**, 015001 (2018).
 - [8] S.-Y. Yang, H. Yang, E. Derunova, S. S. P. Parkin, B. Yan, and M. N. Ali, Symmetry demanded topological nodal-line materials, *Advances in Physics: X* **3**, 1414631 (2018).
 - [9] J. Gooth, A. C. Niemann, T. Meng, A. G. Grushin, K. Landsteiner, B. Gotsmann, F. Menges, M. Schmidt, C. Shekhar, V. Süß, R. Hühne, B. Rellinghaus, C. Felser, B. Yan, and K. Nielsch, Experimental signatures of the mixed axial-gravitational anomaly in the Weyl semimetal NbP , *Nature* **547**, 324 (2017).
 - [10] D. Wawrzik, J.-S. You, J. I. Facio, J. Van Den Brink, and I. Sodemann, Infinite berry curvature of weyl fermi arcs, *Physical Review Letters* **127**, 056601 (2021).
 - [11] M. M. Piva, J. Souza, V. Brousseau-Couture, S. Sorn, K. Pakuszewski, J. K. John, C. Adriano, M. Côté, P. Pagliuso, A. Paramekanti, and others, Topological features in the ferromagnetic Weyl semimetal CeAlSi : Role of domain walls, *Physical Review Research* **5**, 013068 (2023).
 - [12] D. Jérôme, T. M. Rice, and W. Kohn, Excitonic Insulator, *Physical Review* **158**, 462 (1967).
 - [13] W. Kohn, Excitonic phases, *Physical Review Letters* **19**, 439 (1967), publisher: APS.
 - [14] J. M. Blatt, K. Böer, and W. Brandt, Bose-Einstein condensation of excitons, *Physical Review* **126**, 1691 (1962), publisher: APS.
 - [15] V. N. Kotov, B. Uchoa, V. M. Pereira, F. Guinea, and A. Castro Neto, Electron-electron interactions in graphene: Current status and perspectives, *Reviews of modern physics* **84**, 1067 (2012), publisher: APS.
 - [16] J. Kuneš, Excitonic condensation in systems of strongly correlated electrons, *Journal of Physics: Condensed Matter* **27**, 333201 (2015), publisher: IOP Publishing.
 - [17] Y. Jia, P. Wang, C.-L. Chiu, Z. Song, G. Yu, B. Jäck, S. Lei, S. Klemenz, F. A. Cevallos, M. Onyszczyk, N. Fishchenko, X. Liu, G. Farahi, F. Xie, Y. Xu, K. Watanabe, T. Taniguchi, B. A. Bernevig, R. J. Cava, L. M. Schoop, A. Yazdani, and S. Wu, Evidence for a monolayer excitonic insulator, *Nature Physics* **18**, 87 (2022), publisher: Nature Publishing Group.
 - [18] J. Hu, Z. Tang, J. Liu, Y. Zhu, J. Wei, and Z. Mao, Nearly massless Dirac fermions and strong Zeeman splitting in the nodal-line semimetal ZrSiS probed by de Haas-van Alphen quantum oscillations, *Physical Review B* **96**, 045127 (2017).
 - [19] C.-L. Zhang, Z. Yuan, Q.-D. Jiang, B. Tong, C. Zhang, X. Xie, and S. Jia, Electron scattering in tantalum monoarsenide, *Physical Review B* **95**, 085202 (2017).
 - [20] C. Zhang, C. Guo, H. Lu, X. Zhang, Z. Yuan, Z. Lin, J. Wang, and S. Jia, Large magnetoresistance over an extended temperature regime in monophosphides of tantalum and niobium, *Physical Review B* **92**, 041203 (2015).
 - [21] R. Singha, A. Pariari, B. Satpati, and P. Mandal, Magnetotransport properties and evidence of a topological in-

- ulating state in LaSbTe, *Physical Review B* **96**, 245138 (2017).
- [22] F. F. Tafti, Q. D. Gibson, S. K. Kushwaha, N. Haldolaarachchige, and R. J. Cava, Resistivity plateau and extreme magnetoresistance in LaSb, *Nature Physics* **12**, 272 (2016).
- [23] S. Sun, Q. Wang, P.-J. Guo, K. Liu, and H. Lei, Large magnetoresistance in LaBi: origin of field-induced resistivity upturn and plateau in compensated semimetals, *New Journal of Physics* **18**, 082002 (2016).
- [24] F. Fallah Tafti, Q. Gibson, S. Kushwaha, J. W. Krizan, N. Haldolaarachchige, and R. J. Cava, Temperature-field phase diagram of extreme magnetoresistance, *Proceedings of the National Academy of Sciences of the United States of America* **113**, E3475 (2016).
- [25] R. Singha, A. K. Pariari, B. Satpati, and P. Mandal, Large nonsaturating magnetoresistance and signature of nondegenerate Dirac nodes in ZrSiS, *Proceedings of the National Academy of Sciences* **114**, 2468 (2017).
- [26] Y. Wang, L. Thoutam, Z. Xiao, J. Hu, S. Das, Z. Mao, J. Wei, R. Divan, A. Luican-Mayer, G. Crabtree, and others, Origin of the turn-on temperature behavior in WTe₂, *Physical Review B* **92**, 180402 (2015).
- [27] D. V. Khveshchenko, Magnetic-Field-Induced Insulating Behavior in Highly Oriented Pyrolytic Graphite, *Physical Review Letters* **87**, 206401 (2001).
- [28] X. Du, S.-W. Tsai, D. L. Maslov, and A. F. Hebard, Metal-insulator-like behavior in semimetallic bismuth and graphite, *Physical review letters* **94**, 166601 (2005).
- [29] I. A. Luk'yanchuk and Y. Kopelevich, Dirac and normal fermions in graphite and graphene: Implications of the quantum Hall effect, *Physical review letters* **97**, 256801 (2006).
- [30] Z. Zhu, H. Yang, B. Fauqué, Y. Kopelevich, and K. Behnia, Nernst effect and dimensionality in the quantum limit, *Nature Physics* **6**, 26 (2010).
- [31] K. Ziegler, Quantum transport in 3D Weyl semimetals: Is there a metal-insulator transition?, *The European Physical Journal B* **89**, 268 (2016).
- [32] L. Romaka, Y. Dovgalyuk, V. V. Romaka, I. Lototska, and Y. Stadnyk, Interaction of the components in Y-Ni-Sn ternary system at 770 K and 670 K, *Intermetallics* **29**, 116 (2012).
- [33] C. P. Sebastian and R. Pöttgen, The Stannides YNi_xSn₂ (x = 0, 0.14, 0.21, 1) – Syntheses, Structure, and ¹¹⁹Sn Mössbauer Spectroscopy, *Monatshefte für Chemie - Chemical Monthly* **5**, 381 (2007).
- [34] L. Komarovskaya, L. Aksel'rud, and R. Skolozdra, Crystal Structure of the Compound LuNiSn₂ and Its Analogs, *Kristallografiya* **28**, 1201 (1983).
- [35] R. Skolozdra, L. Komarovskaya, and L. Aksel'rud, Magnetic susceptibility of RNiSn₂ and RNi₃Sn₂ compounds (R-rare earths), *Izvestiya Akademii Nauk SSSR, Neorganicheskie Materialy* **24**, 1490 (1988).
- [36] R. Skolozdra, S. Sadykov, L. Komarovskaya, and O. Kuvandikov, Magnetic susceptibility and crystal structure of RNi_{1-x}Sn_{2-y} (R-La, Ce, Pr, Nd, Sm), *Fiz. Met. Metalloved.* (USSR) **65** (1988).
- [37] V. Pecharsky, K. Gschneidner Jr, and L. Miller, Low-temperature heat capacity and magnetic properties of the RNiX₂ compounds (R= La, Ce; X= Si, Ge, Sn), *Physical Review B* **43**, 10906 (1991).
- [38] C. Kittel, *Introduction to solid state physics*, 8th ed. (John Wiley & sons, inc, Hoboken, NJ, 2005).
- [39] J. Eisenstein, Superconducting Elements, *Reviews of Modern Physics* **26**, 277 (1954).
- [40] R. Sankar, G. Peramaiyan, I. P. Muthuselvam, S. Xu, M. Z. Hasan, and F. C. Chou, Crystal growth and transport properties of Weyl semimetal TaAs, *Journal of Physics: Condensed Matter* **30**, 015803 (2018).
- [41] W. A. Roger, J. A. Rowlands, and S. B. Woods, The Fermi surface of white tin using ultrasonic quantum oscillations, *Journal of Physics F: Metal Physics* **6**, 315 (1976).
- [42] M. M. Finkelstein, Fermi surface deformation parameters and cyclotron effective masses in white tin, *Journal of Low Temperature Physics* **14**, 287 (1974).
- [43] D. Shoenberg, *Magnetic Oscillations in Metals* (Cambridge University Press, 1984).
- [44] L. Li, K. Wang, D. Graf, L. Wang, A. Wang, and C. Petrovic, Electron-hole asymmetry, Dirac fermions, and quantum magnetoresistance in BaMnBi₂, *Physical Review B* **93**, 115141 (2016).
- [45] F. Le Mardelé, J. Wyzula, I. Mohelsky, S. Nasrallah, M. Loh, S. Ben David, O. Toledano, D. Tolj, M. Novak, G. Eguchi, S. Paschen, N. Barišić, J. Chen, A. Kimura, M. Orlita, Z. Rukelj, A. Akrap, and D. Santos-Cottin, Evidence for three-dimensional Dirac conical bands in TlBiSSe by optical and magneto-optical spectroscopy, *Phys. Rev. B* **107**, L241101 (2023).
- [46] P. D. Grigoriev, Longitudinal interlayer magnetoresistance in strongly anisotropic quasi-two-dimensional metals, *Physical Review B* **88**, 054415 (2013).
- [47] A. A. Sinchenko, P. D. Grigoriev, P. Lejay, and P. Monceau, Linear magnetoresistance in the charge density wave state of quasi-two-dimensional rare-earth tritellurides, *Physical Review B* **96**, 245129 (2017).
- [48] P. S. Alekseev, A. P. Dmitriev, I. V. Gornyi, and V. Y. Kachorovskii, Strong magnetoresistance of disordered graphene, *Physical Review B* **87**, 165432 (2013).
- [49] G. Vasileva, P. Alekseev, Y. Vasilyev, A. Dmitriev, V. Kachorovskii, D. Smirnov, H. Schmidt, and R. Haug, Magnetoresistance of Monolayer Graphene With Short-Range Disorder, *physica status solidi (b)* **256**, 1800525 (2019).
- [50] J. Feng, Y. Pang, D. Wu, Z. Wang, H. Weng, J. Li, X. Dai, Z. Fang, Y. Shi, and L. Lu, Large linear magnetoresistance in Dirac semimetal Cd₃As₂ with Fermi surfaces close to the Dirac points, *Phys. Rev. B* **92**, 081306 (2015), publisher: American Physical Society.
- [51] S. Komiyama, H. Hirai, M. Ohsawa, Y. Matsuda, S. Sasa, and T. Fujii, Inter-edge-state scattering and nonlinear effects in a two-dimensional electron gas at high magnetic fields, *Phys. Rev. B* **45**, 11085 (1992), publisher: American Physical Society.
- [52] B. Zheng, M. Schulz, and S. Trimper, Dynamic simulations of the Kosterlitz-Thouless phase transition, *Phys. Rev. E* **59**, R1351 (1999), publisher: American Physical Society.
- [53] A. Dmitriev, M. Dyakonov, and R. Jullien, Anomalous Low-Field Classical Magnetoresistance in Two Dimensions, *Phys. Rev. Lett.* **89**, 266804 (2002), publisher: American Physical Society.